PRAMANA
— journal of
physics

Vol. 77, No. 4
October 2011
pp. 611–626

Detection of a periodic structure embedded in surface roughness, for various correlation functions

V C VANI[1,*] and S CHATTERJEE[2]

[1]Department of Instrumentation and Applied Physics, Indian Institute of Science, Bangalore 560 012, India
[2]Indian Institute of Astrophysics, Bangalore 560 034, India
*Corresponding author. E-mail: vani@isu.iisc.ernet.in

MS received 6 January 2011; revised 1 April 2011; accepted 15 April 2011

Abstract. This paper deals with surface profilometry, where we try to detect a periodic structure, hidden in randomness using the matched filter method of analysing the intensity of light, scattered from the surface. From the direct problem of light scattering from a composite rough surface of the above type, we find that the detectability of the periodic structure can be hindered by the randomness, being dependent on the correlation function of the random part. In our earlier works, we had concentrated mainly on the Cauchy-type correlation function for the rough part. In the present work, we show that this technique can determine the periodic structure of different kinds of correlation functions of the roughness, including Cauchy, Gaussian etc. We study the detection by the matched filter method as the nature of the correlation function is varied.

Keywords. Matched filter; rough surface; detection.

PACS Nos 42.25.Fx; 42.30.Kq; 42.30.Sy

1. Introduction

The detection of a surface periodic structure buried in randomness is both an important and a difficult problem. The problem becomes more complicated if either the effect of the randomness increases or the amplitude of the periodic part decreases, making the signal relatively weak.

We use here, the matched filter method for analysing the intensity of the scattered light. We briefly introduce the strategy of the matched filter method as follows. If the surface under study is composed of a periodic part, hidden behind randomness, the scattered intensity will consist of peaks, located periodically, while the peaks will be broadened due to the background of randomness. This is given in §§2 and 3 which deal with the direct problem. The matched filter method, introduced below, is a procedure, in which we search in the scattered intensity of light for a sequence of peaks, that are identically shaped but are of varying amplitudes. We explore here, problems with high randomness, i.e. peaks which are

DOI: 10.1007/s12043-011-0140-1; ***e*Publication: 30 September 2011**

partially overlapping with each other, so that the higher-order peaks, appearing on either side of the central one are subsumed by the central maxima. The strategy here, follows the following steps: (a) anticipate the shapes of the peaks, (b) numerically subtract the contribution from the strongest peak, (c) examine the shapes of the accompanying side lobes and (d) justify, in the 'least square sense' the best case, where the subtracted central peak has the same shape as those of the residual side lobes.

The best fit for the shape of the peaks being thus found, one then tries to extract the locations and the amplitudes of the peaks. In the numerical cases, studied by us, the amplitude a of the periodic part of the random surface is very small. The intensity distribution of the scattered radiation may look very similar to that for the $a = 0$ case. It thus becomes necessary to distinguish between the two cases, i.e. $a = 0$ and $a = a_{\text{matched}}$ (value of a obtained by matched filter analysis). This method is completed by performing the statistical tests, which distinguish between the two competing cases.

Matched filter can be applied to any problem involving scattering from a random surface having hidden periodic structures. Some of the fields where this technique can be used are in medical imaging, in astrophysics for detecting very low angular separation between astronomical objects like binary stars, in spectroscopy, for resolving two closely spaced spectral lines, like Zeeman lines. There are different applications, depending on the field of interest.

We have already shown [1–11] that by the present method, detection of the various peaks of a periodic structure is possible up to $(r_0/\Lambda) \sim 0.11$, where r_0 is the coherence length of the scattered radiation due to the random part of the surface and Λ is the wavelength of the periodic part of the surface. We have studied the usefulness of the method of Cauchy type correlation function of the randomness and for different values for the amplitude a of the periodic structure. We have already discussed and shown by simulation studies [11] that for a given randomness, detection is easier for increasing amplitudes of the periodic structure. The aim of this work is to test the capability of the matched filter as the nature of the surface roughness changes, i.e. as the form of the correlation function of the surface roughness changes. We apply the matched filter analysis technique for different cases of correlation functions of the randomness. The results presented here give us information about the capabilities and limitations of the matched filter technique.

In the following, we first explain the theory behind the matched filter method. We follow this with an extension of the technique for different types of rough surfaces. The difference between the correlation function and the von Karman type of correlation function is discussed in the next section. The results of computer fits, for different types of randomness, follow next and we end the paper with our discussion and conclusions on the merits of this type of analysis.

2. Theory

Let us consider a plane surface, in which the elevations in the z direction are given by

$$\xi(x, y) = a\cos(Qx) + \delta\xi(x, y), \tag{1}$$

where $\delta\xi(x, y)$ denotes the random part, with the average and correlation being

$$\langle \delta\xi(x, y)\rangle = 0, \quad \langle \delta\xi(x, y) \times \delta\xi(x', y')\rangle = \sigma^2 p(r), \quad p(r) = \exp[-(r/l)^\beta], \tag{1.1}$$

where the form for $p(r)$ is an assumption in the modelling of the randomness. In expression (1.1), the symbol $\langle \cdots \rangle$ denotes the average of the quantity inside the bracket, for all possible realizations of the randomness and the separation between the points (x, y) and (x', y') on the surface is given by $r = [(x - x')^2 + (y - y')^2]^{1/2}$. In eq. (1.1) σ gives a measure of the typical elevation due to the randomness and we have chosen the correlation function $p(r)$ to be such that $p(0) = 1$ and $p(r) \to 0$ for $(r/l) \gg 1$, where l is the correlation length of the randomness on the surface while σ is a measure of the standard deviation of the random elevations on the surface. The correlation length l tells us about the length beyond which the randomness get uncorrelated and the exponent β describes, as to how fast the decorrelation of the randomness occurs. The scattering geometry of the scattering surface is given in figure 1.

We define [12,13], the wave vector **v** of scattering to be

$$\begin{aligned} v_x &= k(\sin\theta_1 - \sin\theta_2 \cos\theta_3), \quad v_y = -k \sin\theta_2 \sin\theta_3, \\ v_z &= -k(\cos\theta_1 + \cos\theta_2), \quad v_{xy}^2 = v_x^2 + v_y^2. \end{aligned} \tag{2}$$

In what follows, we shall calculate the scattered intensity under the Kirchoff approximation, which is valid for $4\pi r_c \cos\theta \gg \lambda$, r_c being the typical radius of curvature of the surface [1,2]. Following Beckman and Spizzichino [12] and Beckmann [13], we define a quantity $\langle \rho\rho^* \rangle_0$ to be as follows. Let $I(\mathbf{v})_{\text{rough}}$ be the intensity of the light scattered in the **v** direction by the surface as given in (1) and let $I(\mathbf{0})_{\text{smooth}}$ be the intensity of light scattered along the specular direction ($\mathbf{v} = \mathbf{0}$) for a perfectly smooth surface ($a = 0$ and $\delta\xi(x, y) = 0$ identically), for the same value of the incident intensity. In that case $\langle \rho\rho^* \rangle_0$ is defined as

$$\langle \rho\rho^* \rangle_0 = I(\mathbf{v})_{\text{rough}} / I(\mathbf{v} = \mathbf{0})_{\text{smooth}}.$$

As is clear, for a perfectly smooth surface, the entire intensity is scattered along the specular direction, $\mathbf{v} = \mathbf{0}$, i.e. $\theta_2 = \theta_1$, $\theta_3 = 0$. It can be shown that, for a surface profile as given

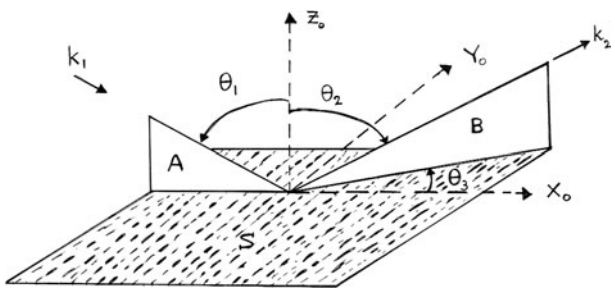

Figure 1. Scattering geometry as used in the paper.

in (1), under the Kirchhoff approximation, for a scalar wave (i.e., ignoring the polarization effects) we have

$$\langle \rho^* \rho \rangle_0 = \left\{ J_0^2(\sqrt{(2g_1)}) f(v_x, v_y; g) + \sum_{n=1}^{\infty} J_n^2(\sqrt{(2g_1)}) \times [f(v_x + nQ, v_y; g) + f(v_x - nQ, v_y; g)] \right\} \times B(\theta_1, \theta_2), \tag{3}$$

where $\sqrt{g} = \sigma v_z/\sqrt{2}$ and $\sqrt{g_1} = a v_z/\sqrt{2}$ (i.e. the dimensionless quantities, $\sqrt{g}$ and $\sqrt{g_1}$ scale the depth of the random elevations and the amplitude of the periodic part to the wavelength of the incident light) and we have defined,

$$f(v_x, v_y; g) = (2\pi/A) \left\{ \int_0^{\infty} \exp(-g[1 - p(r)]) J_0(v_{xy} r) r \, \mathrm{d}r \right\}, \tag{4}$$

where A is the area of the surface in the xy plane,

$$B(\theta_1, \theta_2) = [F_3(\theta_1, \theta_2, \theta_3)]^2 S(\theta_1, \theta_2) \tag{5}$$

$$F_3(\theta_1, \theta_2; \theta_3) = \frac{(1 + \cos\theta_1 \cos\theta_2 - \sin\theta_1 \sin\theta_2 \sin\theta_3)}{(\cos\theta_1(\cos\theta_1 + \cos\theta_2))} \tag{6}$$

$$S(\theta_1, \theta_2) = S(\theta_1) S(\theta_2) \tag{7}$$

with

$$S(\theta) = \exp\big[(-1/4) \tan\theta \operatorname{erfc}(K \cot\theta)\big] \tag{8}$$

$$K^2 = (aQ)^2 + 4(\sigma/l)^2 \tag{9}$$

of which $F_3(\theta_1, \theta_2; \theta_3)$ is a geometrical factor and $S(\theta_1, \theta_2)$ describes the 'shadowing effect'.

3. Intensities for different roughness situations

For strong roughness, we have $g \gg 1$ and we can thus approximate

$$\exp(-g[1 - p(r)]) \approx \exp[-(r/r_0)^{\beta}], \tag{10}$$

where $r_0 = l/g^{1/\beta}$. This indicates that for the same values of l and g the correlation length r_0 is smaller for larger β, for $g \gg 1$. It can be seen that on using the approximation, given in (10), the quantity $f(v_x, v_y; g)$ will have the form,

$$f(v_x, v_y; g) = (2\pi/A) \left\{ \int_0^{\infty} \exp[-(r/r_0)^{\beta}] J_0(v_{xy} r) r \, \mathrm{d}r \right\}, \tag{11}$$

$$= (2\pi/A)(r_0^2) \left\{ \int_0^{\infty} \exp[-z^{\beta}] J_0(v_{xy} r_0 z) z \, \mathrm{d}z \right\}, \tag{12}$$

where $z = (r/r_0)$ and we denote from now on, $\alpha = v_{xy} r_0$.

The exact form for the above integral is known only for $\beta = 1$ and 2. For all other cases approximations are to be made, while exploiting the exact, known values of the integrals, as given in the above cases. We shall now on deal with the case $v_y = 0$ so that $v_{xy} = v_x$ and also assume that barring some multiplicative constants,

$$f_a(v_x) = \left[1 + (c/2y)\, v_x^2\right]^{-y}, \tag{13}$$

where the values of c and y (in terms of r_0 and β) are given in eqs (A.4) and (A.5) in the Appendix. We justify this approximation (13) for $f(v_x)$, by comparing the exact values of the integral in (12) with the values that we obtain on using expressions (13), (A.4) and (A.5). Figure 2 proves the correctness of this choice of approximation. It is further seen

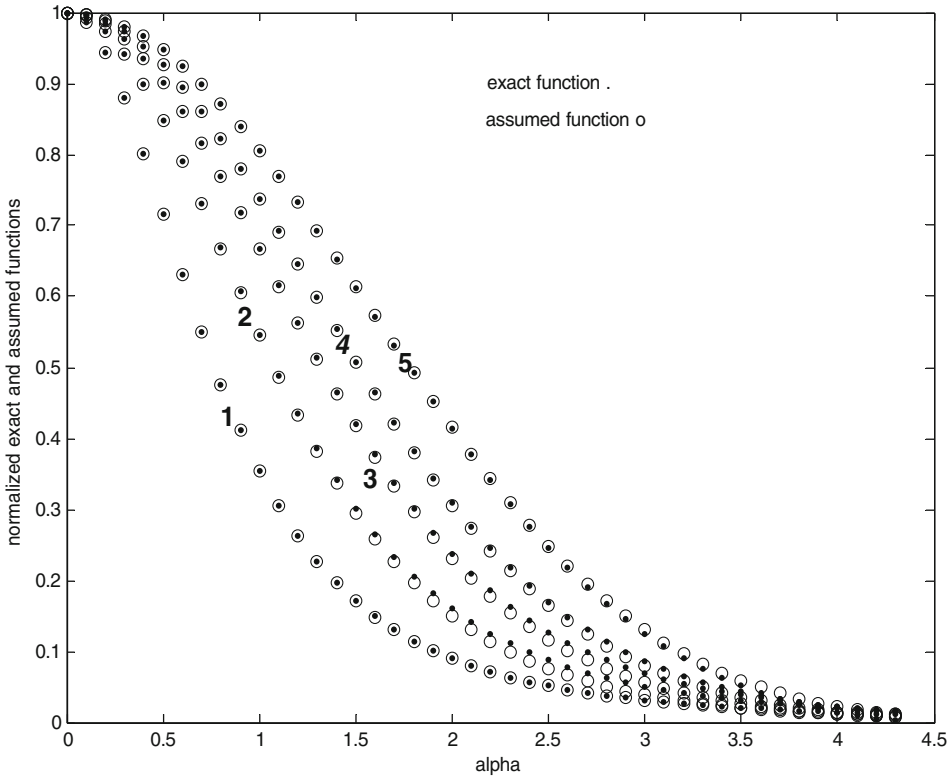

Figure 2. A plot of alpha ($\alpha = v_x r_0$) vs. the normalized values of the exact function $f(v_x)$ and the assumed function $f_a(v_x)$. The exact function $f(v_x)$ is denoted by points, as obtained by numerically integrating the expression given in (12), between $z = 0$ and 4, in steps of 0.001 and the assumed function $f_a(v_x)$, as given by (13) is denoted by $\circ$. Each curve represents a fixed β value, i.e., 1.0, 1.25, 1.5, 1.75 and 1.95, and is represented by the curves, 1, 2, 3, 4 and 5 respectively. We find in figure 2, the extremely good agreement between the exact and assumed values of the function $f(v_x)$ and for different values of β. In all cases $r_0 = 2.024 \times 10^{-4}$.

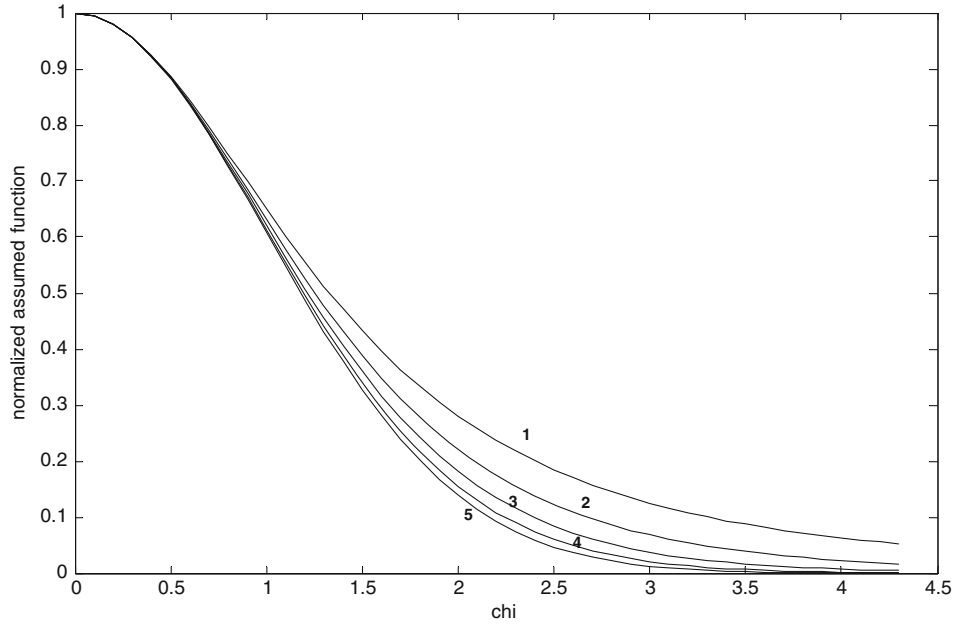

Figure 3. The plot of $\chi (= c^{1/2}/v_x)$ vs. the normalized values of the assumed function $f_a(v_x)$, as given by (13). The relation between r_0 and c, y and β is given in eqs (A.5), (A.6) in the Appendix. Each curve represents a fixed β value, i.e., $\beta = 1.0$, 1.25, 1.5, 1.75 and 1.95, and is represented by the curves, 1, 2, 3, 4 and 5 respectively, with the corresponding y values being 1.5, 2.80, 5.45, 13.43 and 77.42. It is to be noted that the curvature of the curves at the origin for all the curves is the same but the curves tend to be sharper as the exponent β increases.

that given the quantity $f''(0) = c$ for all the curves, their curvature at the origin is the same but the randomness with higher value of β gives rise to a sharper fall in the functions $f(v_x)$ and $f_a(v_x)$. This implies that for the same value of c, the detectability is more difficult for a lower value of β (figure 3).

A detectability criterion can be easily derived from eq. (3). In these discussions we shall consider $f(v_x)$ to have the form

$$f(v_x) = f_a(v_x) = \left[1 + (c/2y)v_x^2\right]^{-y}. \tag{14}$$

The parameters c and y, in the function $f(v_x)$, are determined using the values of the wavelength of the incident light (λ), the correlation length (l), the randomness given by σ and the nature of randomness given by β. The different Bessel functions depend on the amplitude a of the periodic part. Given these dependencies, we study the matched filter detection as functions of various values of c, y, a and Q. We have earlier carried out a similar study for $y = 1.5$ when $\beta = 1.0$, i.e. for the Cauchy case, while for $\beta = 2.0$, i.e. the Gaussian case, we have $y \to \infty$, i.e. $f(v_x)$ also turns out to be Gaussian. In the present work we shall numerically study different cases, particularly emphasizing the role the exponent y plays in the detection.

The complete expression for the intensity in our simulation procedure is thus given by

$$\begin{aligned}\langle \rho^* \rho \rangle_0 &= [\text{Intensity of scattered light, in the direction } v] \\ &= J_0^2 (a v_z) [1 + (c/2y) v_x^2]^{-y} \\ &\quad + \sum_{n=1}^{\infty} J_n^2 (a v_z) \cdot [1 + (c/2y)(v_x \pm nQ)^2]^{-y}. \end{aligned} \tag{15}$$

We use eq. (11) in all our numerical simulations, and simulate $\langle \rho^* \rho \rangle_0$ for some selected values of y and c. We then try to see whether the matched filter method succeeds in obtaining the correct values for the parameters a and Q, in every case of the specified randomness. This will give us information about the matched filter fits, its applicability and also its limitations.

Since the ratio (a/λ) is small, the central peak, given by the J_0^2 term dominates over the successive peaks, which vary as J_n^2. Also since we choose the cases where $(r_0/\Lambda) \ll 1$, the central peak also subsumes the higher-order peaks. The consequent result is that only the zeroth-order peak is seen and it will be very wide, smearing out all other peaks. The matched filter detection procedure removes the lower-order (thus the stronger) peaks from the scattered light intensity (known to us) and thus helps to detect the next order peak, a process to be undertaken step by step. This procedure ensures the detection of the highest-order peak in the remaining data and makes the detection of all the peaks simpler. The interested reader can find a detailed explanation in [1–11]. The present paper deals with this case for different values of (a/λ) and (r_0/Λ) and y (which describes the tail regions of different peaks) and also tries to explore the applicability of the matched filter method when these parameters are changed.

4. Relation with the von Karman correlation spectrum

From the definition of the correlation function, it is seen that the structure function of the rough part is given by

$$D_{\xi\xi}(\mathbf{r}, \mathbf{r}') = \langle |\xi(\mathbf{r}) - \xi(\mathbf{r}')|^2 \rangle = \sigma^2 [p(\mathbf{0}) - p(|\boldsymbol{\rho}|)], \tag{16}$$

where $\boldsymbol{\rho} = (\mathbf{r},\mathbf{r}')$. Thus from the above, we can approximate for $|\boldsymbol{\rho}| \to 0$,

$$\begin{aligned}\langle |\xi(\mathbf{r}) - \xi(\mathbf{r}')|^2 \rangle = \sigma^2 [p(\mathbf{0}) - p(|\boldsymbol{\rho}|)] &= \sigma^2 ((|\boldsymbol{\rho}|/l)^{\beta}) \\ &= \langle (\partial \xi(\mathbf{r})/\partial \mathbf{r})^2 \rangle \, |\boldsymbol{\rho}|^2 . \end{aligned} \tag{17}$$

This shows that we should have

$$\langle (\partial \xi(\mathbf{r})/\partial \mathbf{r})^2 \rangle = \sigma^2 \, |\boldsymbol{\rho}|^{\beta - 2} \, (l)^{\beta} . \tag{18}$$

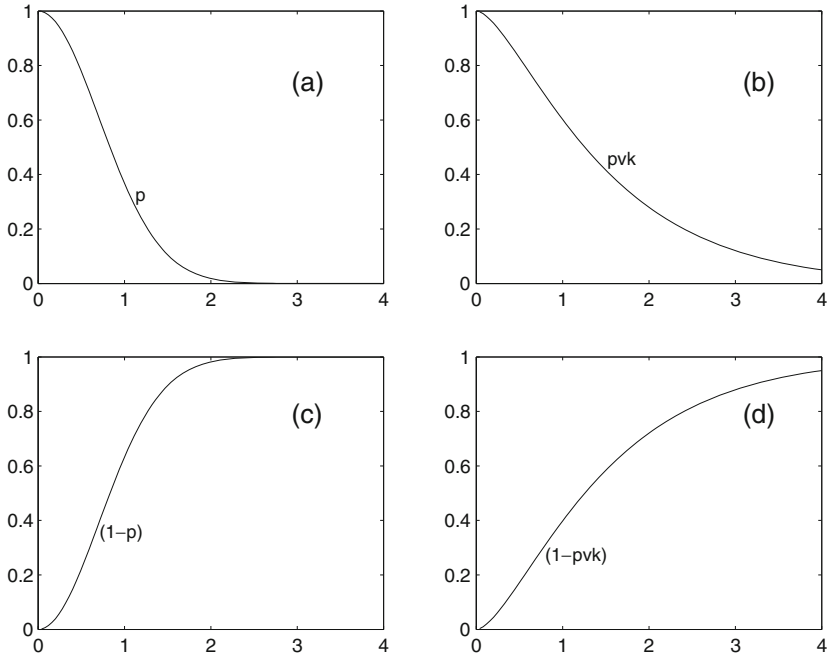

Figure 4. Plots of the correlation functions used in the matched filter calculations and the von Karman correlation function. p denotes the function used in matched filter and pvk represents the von Karman correlation function. The x-axis depicts the values of (r/l). Plots (**a**), (**b**), (**c**) and (**d**) represent p, pvk (vk stands for von Karman), $(1 - p)$ and $(1 - \text{pvk})$.

Thus the gradient of the surface diverges for $\beta < 2$, as can be the case for surfaces with sharp edges or with steep grooves. The latter represents $\beta = 1.0$, i.e. an exponential decay of the correlation function, produced by a 'random telegraph signal' kind of disorder. Many authors consider, the von Karman correlation function, $p_{\text{VK}}(|\boldsymbol{\rho}|) = [2^{v-1}\Gamma(v)]^{-1}\,((|\boldsymbol{\rho}|)/l)^{v}K_v(|\boldsymbol{\rho}|/l)$, while we consider, $p(|\boldsymbol{\rho}|) = \exp[-(|\boldsymbol{\rho}|/l)^{\beta}]$. Our model coincides with the von Karman model in the limit $(|\boldsymbol{\rho}|/l) \to 0$, with $\beta = 2v$. In the opposite limit, our model has a fall as $\exp[-(|\boldsymbol{\rho}|/l)^{\beta}]$, while the von Karman one falls as, $(|\boldsymbol{\rho}|/l)^{v-(1/2)}\exp(-|\boldsymbol{\rho}|/l)$. Their differences in the $(|\boldsymbol{\rho}|/l) \to \infty$ would give rise to light scattering patterns, which differ from each other only in the low-angle scattering regime. However, this difference gets obliterated as the quantity $g \sim (\sigma/\lambda)$ becomes larger and larger. This can be seen as follows. As can be seen, the scattering cross-section is proportional to $f(v_x, v_y, v_z)$, which is a Fourier transform of $F(r) = \exp(-g(1 - p(r)))$. In figure 4 we plot $p(r)$, $p_{\text{VK}}(r)$, $[1 - p(r)]$ and $[1 - p_{\text{VK}}(r)]$, the last two are proportional to the structure function in the two cases. Finally, in figure 5 we plot the quantities, $\exp(-g(1-p(r)))$ and $\exp(-g(1-p_{\text{VK}}(r)))$, for different values of g and find that the two curves come closer to each other as g increases. It thus follows that their Fourier transforms too will differ marginally in such cases.

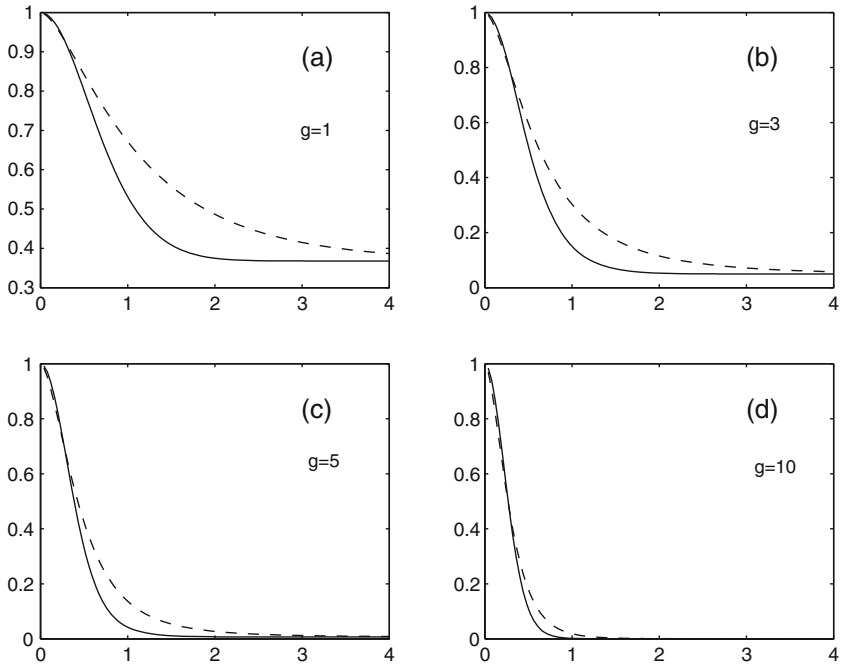

Figure 5. Plot of the functions $F(r)$. Each plot contains two graphs: $F(r) = \exp(-g(1 - p(r))$ (continuous curve) and $F_{\mathrm{VK}}(r) = \exp(-g(1 - p_{\mathrm{VK}}(r)))$ (dashed curve). We find from the plots (**a**) to (**d**) that both the functions become very close to each other, as g increases from 1 to 10.

5. Numerical results

The purpose of this numerical analysis is to show that the matched filter method of analysis is valid for different correlation functions representing different kinds of rough surfaces. The important thing is to reproduce not just the peak but also the tail distribution in the intensity of the scattered light. As is already known, intensity of the scattered light depends on the surface roughness. For the Cauchy kind of distribution, $\beta = 1.0$ and thus $p(r) = \exp(-r/l)$, while $f(v_x) = [1 + (v_x r_0)^2]^{-3/2}$. Thus the fall is quite large till $(v_x r_0) = 1$ and beyond that the fall is slow, being a power law kind of the type, $(v_x r_0)^{-3}$. For the Gaussian case, $p(r) = \exp[(-r/l)^2]$, while $f(v_x) = \exp[-(v_x r_0/2)^2]$, i.e. has a fairly slow fall till $v_x r_0 = 2$ and falls abruptly for higher values of $v_x r_0$. We consider different roughness and show graphically the results of the matched filter analysis.

The procedure for the analysis is as follows. The calculations are carried out for different sets of parameters y, a, c and Q, for $\lambda = 6328$ Å. Intensity values are obtained for each case using eq. (11), which is treated by us as the 'data'. Design of the matched filter follows, involving the characterization of the central or zero-order peak, first-order and second-order peaks of the intensity. The conditions of matching are applied for each case, the basic demands for an acceptable fit being: (1) The higher-order peaks must match with the shape of the central peak and (2) the peaks must be equally spaced.

We begin by assuming that the peaks have the shape, $f_a(v_x) = [1 + c'v_x^2/2y']^{-y'}$ and select the values of c' and y', which satisfy our observed $\langle\rho^*\rho\rangle_0$ profile. This is done for the total intensity profile as well as for the structures contained within this profile.

We start with the parameters c' and y' for designing the matched filter. Matched filter design is derived from the light scattering data from the rough surface. The search for the correct values of c' and y', pertaining to the rough part of the surface, proceeds as follows.

1. The parameters c' and y' are both varied. We do not float both parameters. Instead, we vary both of them in known steps. This procedure has the following advantages: The data fit remains linear, the search procedure is simpler and we reach a unique minimum.
2. We first vary both parameters in a wide range. This is a blind search and is coarse in nature. The results give us an approximate idea about the location of the least square deviation.
3. This next step refines the search. The values of c' and y' are restricted, based on the results of step 2. The best fit values for c and y are found by a method of least squares, satisfying the conditions (1) and (2) stipulated above. Once the parameters c' and y' are fixed, we keep them fixed at their best fit values and search for the values of a and Q. We follow the same procedure as in steps 2 and 3. For every possible choice of a and Q, we calculate the quantity $\langle\rho^*\rho\rangle$, as obtained by (15) and settle for the case, giving the least square in the deviation between the theoretical and the observed values. The result of this procedure is illustrated in figures 6 and 7. The

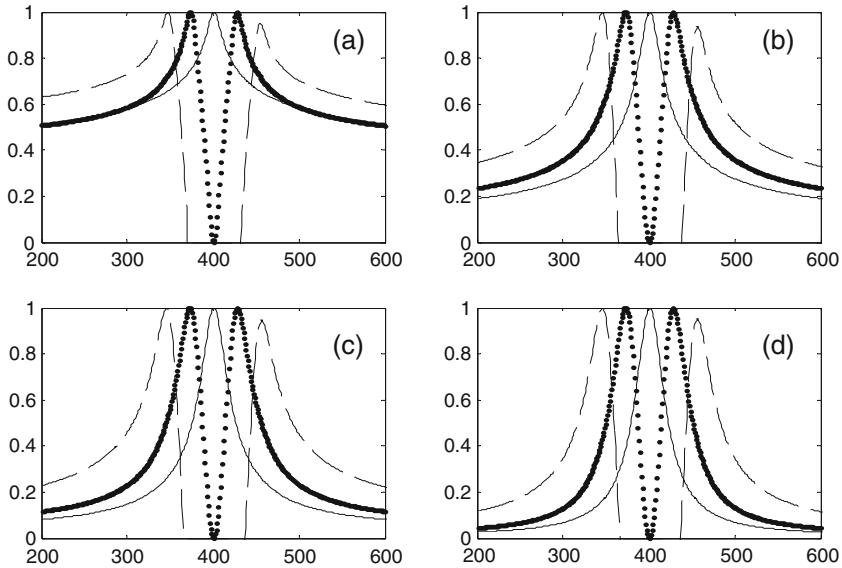

Figure 6. The matched filter reconstruction. The central peak is shown by a continuous line (——), first-order peaks by (· · ·) and second-order peaks by (- - -). (**a**) to (**d**) represent different values of the exponent y. (**a**) $y = 0.1$, (**b**) $y = 0.3$, (**c**) $y = 0.5$, (**d**) $y = 0.8$. Every peak is normalized to its own maximum. In all cases $r_0 = 2.024 \times 10^{-4}$.

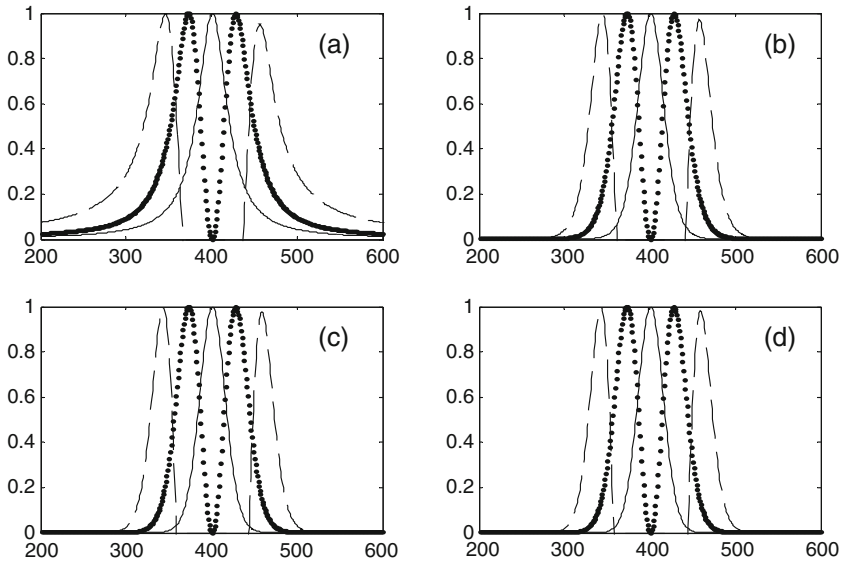

Figure 7. The matched filter reconstruction. The central peak is shown by a continuous line (—), first-order peaks by $(\cdots)$ and second-order peaks by (- - -). (**a**) to (**d**) represent different values of the exponent y. (**a**) $y = 1$, (**b**) $y = 5$, (**c**) $y = 10$, (**d**) $y = 20$. Every peak is normalized to its own maximum. In all cases $r_0 = 2.024 \times 10^{-4}$.

adjustments of c and y are done in such a way, that the side lobes, that are left behind when the central maxima of the type $f_a(v_x)$ is taken away from $\langle \rho^* \rho \rangle$, leaves behind a side lobe, whose shape is the same as that of $f_a(v_x)$. In other words, the accepted values of c and y are those for which the shape of the side lobes also have a form $[1 + (c'/2y)(v_x \pm Q)^2]^{-y'}$. With this choice of c' and y' one then identifies the peaks of the side lobes to be located at $\pm Q$, while the value of a is determined by noting that the height of the side lobes must vary as given by the Bessel function terms in (15) and also retain the shape, as given by the matched filter. Further, once the values of c, y, a and Q are found, the second-order peaks can be found by subtracting out the first two terms of (15) from the data of $\langle \rho^* \rho \rangle$. While c' and y' are fixed, the values of a and Q are fine-tuned to ensure that the first- and second-order lobes match the shape as predicted by the matched filter parameters. These values of the numerically determined parameters match the values with which the simulations were made.

All these four parameters c, y, a and Q together decide the nature of the surface and hence the intensity of the scattered light from the surface. Now, we show with the help of graphs, the scattered intensities and the detection of the various peaks.

As the value of c increases, roughness decreases, peaks become sharper and detection of the various peaks is possible even at a lower amplitude of periodicity a. (There is also the exponent involved, deciding the rate of fall of the correlation.) Higher the value of the exponent, detection of the buried signal is easier, since the tail region falls faster. Amplitude of the signal a determines the values taken by the Bessel functions, and hence gives us the amplitude of the peaks, while the wave vector of the periodic part Q determines the

position of the various peaks. The effect of all these parameters determines the capability of the matched filter.

Matched filter reproduction in various cases, involving various values of the parameters are shown below. We consider mainly the role of the parameters c and y. Our findings with a, the amplitude of the signal, is already published [11]. Our 'proof' will be in the form of figures and is followed by discussions in the end.

Figures 6 and 7 show the matched filter fits for a fixed value of $c = 3 \times 10^{-8}$ and the exponent y varying from 0.1 to 20.

In figure 6 we find that when the exponent is 0.1 or 0.3, the tail regions are not well reproduced. This value can be taken as the limit of the matched filter method of data analysis. In figures 6c and d, where the exponent takes the value 0.5 and 0.8, the reproduction is fair. The fact that for smaller values of y, detection becomes difficult, results from the behaviour in the tail of $f(v_x)$ as y is made smaller. When y reduces, the shape of $f(v_x)$ becomes wide and hence the peaks cannot be separated out.

It is further seen from figure 7 that as the exponent y increases, the fall of $f(v_x)$ is quite abrupt. This sharpness in $f(v_x)$ makes the detection easier. A Gaussian profile for the correlation function yields a Gaussian profile for the peaks too, and the absence of long tails in these Gaussian profiles thus aids detection. Considering the good fits given by the matched filter for exponents upwards of 0.5, we conclude that the matched filter technique

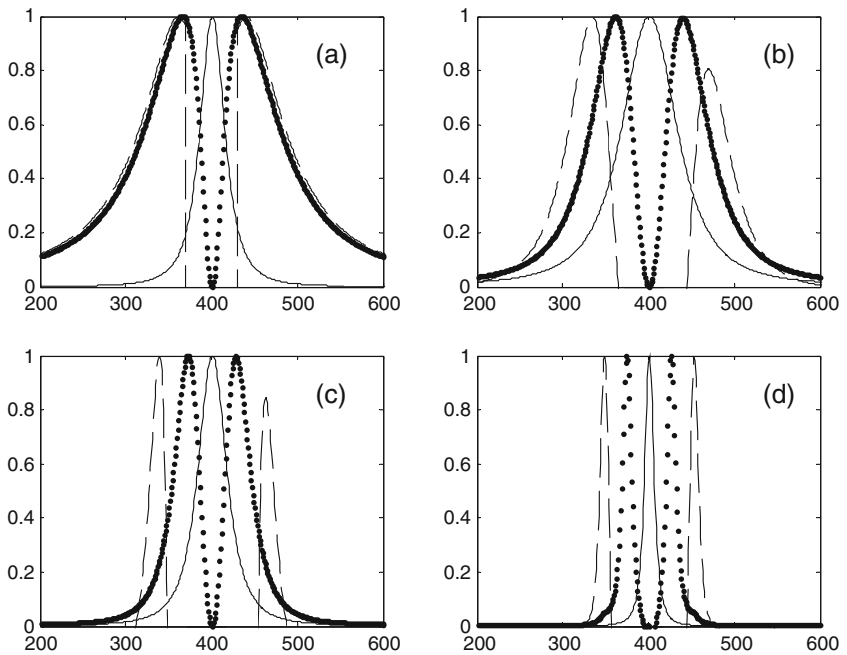

Figure 8. The matched filter reconstruction. The central peak is shown by a continuous line (——), first-order peaks by (· · ·) and second-order peaks by (- - -). (**a**) to (**d**) represent different values of c. $y = 1.5$ in all cases. (**a**) $c = 3.0 \times 10^{-9}$, (**b**) $c = 8.0 \times 10^{-9}$, (**c**) $c = 3.0 \times 10^{-8}$ and (**d**) $c = 3.0 \times 10^{-7}$. Every peak is normalized to its own maximum.

is quite capable to 'see through' even long tails, a result which we had not anticipated in our previous works.

Figure 8 shows the quality of the matched filter detection for various values of c.

As the roughness decreases, the parameter c increases and detection of the periodic structure becomes easier, and after the roughness increases beyond a certain level (in this case represented by $c = 3 \times 10^{-9}$ and $y = 1.5$), the matched filter cannot detect the periodic signal anymore. This detection regime is found to be much wider than what would be given if the conventional methods were followed (i.e. merely to look for peaks in the scattered intensities). The matched filter methods make the peaks 'revealing', which the conventional methods fail to do. The basic issues related to this question are addressed in ref. [11], which the interested reader may refer to.

The choice of $y = 1.5$ was made in many of our investigations, to model a roughness, produced by grooves of height σ but of various widths. The number of grooves per unit length is considered to follow a Poisson statistics, there being on an average $(1/l)$ grooves per unit length. As y approaches infinity, we are dealing with a random surface, whose curvature is a well-defined quantity. In all our computations, we have chosen c and y in such a way that all the higher-order peaks are submerged in the central maxima. We define the detectability regime to be the region in the (c, y, Λ, a) space, where the usual intensity profile shows up the peaks in the intensity. In an earlier paper, we had investigated the regime of detectability in the (c, y, Λ, a) parameter space. In the present paper, we have chosen the above parameters to lie in the non-detectabilty range, to demonstrate the usefulness of the present method. This helps us also to understand as to what extent the present method is capable of meeting the demands.

In all our fits $r_0 = 2.024 \times 10^{-4}$. β values are mentioned in the figure caption for the relevant figures. The value of r_0 is decided by the quantities σ, l, β and λ, which combine to give the quantities c and y. Also, since r_0 scales as the width of the peaks, presenting a plot in terms of $r_0 v_x$ will not add to the information obtained from the plot.

6. Discussion

We have examined the capability of the matched filter detection technique for different values of c and y that appear in the expression for $f(v_x)$. Given that the search for the correct shape of $f(v_x)$ is extremely important for the detection of hidden periodicity, we have developed an efficient search procedure which very accurately arrives at the matched filter parameters and then proceeds to find the parameters a and Q, which pertain to the hidden periodic part. We have also discussed the limitations of this technique.

When the matched filter gives a very small value of (a/λ), it is necessary to distinguish this case, i.e. $(a/\lambda) \ll 1$, from the case where $(a/\lambda) = 0$. It is seen from the Kolmogorov–Smirnov (KS) and the maximum likelihood (ML) tests, that the case $(a/\lambda) \neq 0$ cannot be statistically distinguished from the one giving $(a/\lambda) = 0$, if the value of (a/λ) falls below a critical value. The way these tests have to be performed to discriminate between the two competing cases, has been dealt with in detail in our earlier work [11] to which an interested reader is referred. The main point is that the KS and ML tests give weightage to the peaks in the probability density function, while we anticipate the differences in the two

cases to appear in the tails of the above function. It is thus clear that while for low values of a, we cannot distinguish this case from the case with $a = 0$, in terms of the total intensity of the scattered light or from the values at the central peak, the case $a = 0$ cannot give rise to side lobe structures of the type shown, which match with each other. This idea has been used by us in [11] and a full scale statistical test has to be developed to rule out $a = 0$ from the $a \neq 0$ case, derived from our matched filter analysis. This has not been done and is being seriously pursued by us, with an idea to give a fool-proof method, for detecting hidden periodicities. Further, the present paper gives valid justification for assuming the function $f_a(v_x)$ to have a form as given in (14). This assumption for light scattering from the rough part of the surface, was made in all our previous works and the validity of this approximation has been proved in the Appendix and in the numerical simulations. This is an important issue, around which the present matched filter method is centred. Earlier, we had shown that the matched filter method is capable of showing up the hidden periodicities for exponents $1.5 \leq y \leq \infty$. In this paper, we show that the lower limit of y for which detection is permitted, can go as low as 0.5, a definite advance over what was anticipated earlier, though the accuracy of the method suffers as y decreases.

The justification of the form of $f(v_x)$, with that given by $f_a(v_x)$ and the dependence of c and y on g and β, as given in eqs (A.5) and (A.6) show the potential of multi-wavelength analysis for the characterization of roughness. The model of the correlation function, used by us can incorporate various kinds of disorders, as are being discussed by various authors [14,15]. As is discussed here, the prospect of the matched filter method depends largely on an accurate knowledge of c and y. The selection of their values would be greatly facilitated if one of them could be known independently. As eq. (A.6) shows, y depends only on β and is thus independent of the wavelength of the light used for observation. Using long-wavelength light makes the J_n^2 terms very small while $J_0^2 \approx 1$ and hence one would have approximately, $\langle \rho^* \rho \rangle \approx f(v_x)$, that would enable one to know the behaviour of $f(v_x)$, as the central peak is not interfered by the higher-order peaks. Once y is determined from the data in the long-wavelength regime, experiments at higher wavelengths could be used to make the higher-order peaks more prominent and thus ascertain the values of a and Q more accurately.

The case $\beta = 1$ corresponds to a random surface, similar to a random telegraph signal. Clearly, surfaces with smaller values of β are rougher. We have not theoretically studied such cases but have presented a case study, with $\beta = 0.1$, 0.3, 0.5 and 0.8 (figure 6) and show that the matched filter method is capable of detecting hidden randomness in such cases too, of course within a more restricted regime in the (c, y, Λ, a) space than would happen for a higher value of β.

The detectabilty of the periodic structure is decided by two dimensionless quantities, $x = Qr_0 = (2\pi r_0/\Lambda)$ and $y' = (a/\lambda)$. The former scales the coherence length r_0 with the wavelength Λ of the periodic part and tells us as to how the width of the peak $\Delta\theta \propto (\lambda/r_0)$ compares with the separation between the peaks, $\delta\theta \propto (\lambda/\Lambda)$. Clearly, the detectability will improve as the peak widths become smaller than the separation between the peaks. Thus a larger value of x helps in detection. The role that y' plays in deciding the detectability, comes from the fact that higher values of (a/λ) reduce the height of the $n = 0$ peak and make the $n = 1, 2, 3...$ peaks to be of lower intensity, their intensities being proportional to $J_n^2(av_z)$. Thus, higher values of $y' = (a/\lambda)$ also facilitate detection. These questions are addressed in our earlier publication and are not repeated here.

We have simulated the intensity 'data' with very small values of $y' = (a/\lambda) \sim 0.00$–$0.095$. The matched filter method thus also yields a small value for the value of a. The intensity, simulated by using this value for a, will thus be very close to the 'data' but so would be the intensity, obtained by using $a = 0$. It is necessary to distinguish between these two cases. The usual tests like the chi-square test and the Kolmogorov–Smirnov test would often fail to distinguish between the two, since these tests put more weightage at the peak of the distribution, while we expect the differences to appear in the tails. We thus introduce two new parameters: $r_{\mathrm{mf}}(v_x) = I_{\mathrm{mf}}(v_x)/I_{\mathrm{data}}(v_x)$ and $r_0(v_x) = I_{\mathrm{mf}}(v_x, a{=}\,0)/I_{\mathrm{data}}(v_x)$, where the suffixes, mf and 0 signify the matched filter case and the $a = 0$ case respectively. We must examine, as to which of the two ratios lies closer to the value 1, throughout the entire range of v_x. In all the cases studied (for all of them $(a/\lambda) \ll 1$), we find the ratio $r_{\mathrm{mf}}(v_x)$ to yield a value closer to 1, consistently, particularly at the tails. Certainly, this method of discrimination would breakdown if (a/λ) is very close to zero. Interested readers may refer to our paper [11].

7. Conclusion

The role of the matched filter in detecting a periodic surface buried in a random background is discussed. The study has dealt with the dependence of our analysis technique on various parameters. The limitations of this technique are also pointed out.

Appendix A

In the present case, we are interested in determining the first and the second peaks, located at $v_x = \pm Q$ and $v_x = \pm 2Q$ respectively. Thus, it would be necessary to know the variation of $f(v_x)$ within this range of v_x,, i.e. v_x lying within $\pm 2Q$. As is known, by conventional methods, the peaks are not detectable for $(r_0/\Lambda) \leq 0.33$, i.e. $2Qr_0 \leq 2(2\pi r_0/\Lambda) = 4.14$, which means that it suffices for us to know the variation of $f(v_x)$ within the range, $v_x r_0 \leq 2Qr_0 = 4.14$, i.e. for values of $v_x r_0$ not too large. This is done by inspecting the variation of $f(v_x)$ by expanding the Bessel function as a power series and integrating.

By expanding the Bessel function in the integral, as a power series,

$$J_0(vr) = \sum [(-1)^n/(n!)^2]\,(vr/2)^{2n} \tag{A.1}$$

we get the integral in (12) to be, equal to

$$\begin{aligned} &\sum [(-1)^n/(n!)^2]\,(v/2)^{2n} \int_0^\infty \exp[-(r/r_0)^\beta] r^{2n+1} \mathrm{d}r \\ &= \left(l^2/\beta\right) \sum [(-1)^n/(n!)^2]\,(vr_0/2)^{2n}\,\Gamma\left((2n+2)/\beta\right), \end{aligned} \tag{A.2}$$

which converges for

$$(v_x r_0/2)^2 \leq \{\Gamma\left((2n+4)/\beta\right)/\Gamma\left((2n+2)/\beta\right)\}\{\Gamma\left(n+1\right)/\Gamma\left(n+2\right)\}^2. \tag{A.3}$$

To approximate the expression for $f(v_x)$, in the form $f_a(v_x) = [1 + (cv_x^2/2y)]^{-y}$, we note that for small values of $(cv_x^2/2y)$,

$$[1 + (cv_x^2/2y)]^{-y} = 1 - (cv_x^2/2) + [y(y+1)/2!](cv_x^2/2y)^2 - \dots . \quad \text{(A.4)}$$

Comparing the first three terms of the above expression with (A.2) we can identify

$$c = (r_0^2/2)\,[\Gamma(4/\beta)/\,\Gamma(2/\beta)] \quad \text{(A.5)}$$

$$y \approx 2[\Gamma(4/\beta)]^2/\,[\Gamma(6/\beta)\Gamma(2/\beta) - 2[\Gamma(4/\beta)]^2]. \quad \text{(A.6)}$$

The above expressions are, in general not exact but give the necessary trends for small values of $(v_x r_0)$. For the special cases of $\beta = 1$ and 2, we get from (A.6) $y = 3/2$ and $y \to \infty$, respectively, which are also the exact closed form expressions for the integral, valid over all ranges of values for $(v_x r_0)$. These results enable us to approximate the envelope of $f(v_x)$ to be as given by the power law, $f_a(v_x) \approx [1 + (cv_x^2/2y)]^{-y}$. The deviation of the exact integral from this approximation will always be small. We examine the form of this approximation with the exact values, given by the exact integral (12) and find the deviations between the two to be extremely small.

References

[1] S Chatterjee, *Indian J. Phys.* **B74**, 363 (2000)
[2] S Chatterjee and V C Vani, *Bull. Astron. Soc. India* **30**, 835 (2002)
[3] S Chatterjee and V C Vani, *J. Mod. Opt.* **50**, 833 (2003)
[4] V C Vani and S Chatterjee, *Bull. Astron. Soc. India* **31**, 457 (2003)
[5] V C Vani and S Chatterjee, *Curr. Sci.* **86**, 177 (2004)
[6] V C Vani and S Chatterjee, *Appl. Opt.* **46**, 3664 (2004)
[7] S Chatterjee and V C Vani, *Pramana – J. Phys.* **65**, 413 (2005)
[8] S Chatterjee and V C Vani, *Third International Conference on Inverse Problems: Modeling and Simulation* (May 29–June 02, 2006)
[9] V C Vani and S Chatterjee, *Appl. Opt.* **45**, 8939 (2006)
[10] V C Vani and S Chatterjee, *Pramana – J. Phys.* **70**, 875 (2008)
[11] V C Vani and S Chatterjee, *Phys. Scr.* **81**, 055402 (2010)
[12] P Beckmann and A Spizzichino, *The scattering of electromagnetic waves from random surfaces* (Pergamon Press, Oxford, 1963)
[13] P Beckmann, Scattering of light by rough surfaces, in: *Progress in optics* edited by E Wolf (North Holland, 1967) Vol. 6, pp. 55–69
[14] Y-P Chao, Irene Wu, C-F Cheng, Ueyn Block, G-C Wang and T M Lu, *J. Appl. Phys.* **84**, 2571 (1998)
[15] Chanfu Chen, Chunxiang Liu, Ningyu Zhang, Tianquing Jia, Ruxin Li and Zhinzhan Lu, *Appl. Opt.* **41**, 2571 (1998)